Thiocyanate-Free Ru(II) Sensitizers with a 4,4′-Dicarboxyvinyl-2,2′-bipyridine Anchor for Dye-Sensitized Solar Cells

Kuan-Lin Wu, Wan-Ping Ku, Sheng-Wei Wang, Aswani Yella, Yun Chi, Shih-Hung Liu, Pi-Tai Chou,* Mohammad K. Nazeeruddin,* and Michael Grätzel**

A new class of thiocyanate-free Ru(II) sensitizers with 4,4′-dicarboxyvinyl-2,2′-bipyridine anchor and two *trans*-oriented pyrid-2-yl pyrazolate (or triazolate) functional chromophores is synthesized, characterized, and evaluated in dye-sensitized solar cells (DSCs). Despite their enhanced red response and absorptivity when compared to the parent sensitizer TFRS-2 that possesses standard 4,4′-dicarboxyl-2,2′-bipyridine anchor and shows the best conversion efficiency of $\eta = 9.82\%$, the newly synthesized carboxyvinyl-pyrazolate sensitizers, TFRS-11–TFRS-13, exhibit inferior performance characteristics in terms of short-circuit current density (J_{SC}), open-circuit voltage (V_{OC}), and power conversion efficiency (η), the latter being recorded to be in the range 5.60–7.62%. The reduction in device efficiencies is attributed to a combination of poor packing of these sensitizers on the TiO_2 surface and less positive ground-state oxidation potentials, which, respectively, increase charge recombination with I_3^- in electrolytes and impede the regeneration of sensitizers by I^- anions. The latter obstacle can be circumvented in part by the replacement of the pyrazolates with triazolates, forming the TFRS-14 sensitizer, which exhibits an improved J_{SC}, V_{OC}, and η of 16.4 mAcm^{-2}, 0.77 V, and 9.02%, respectively.

1. Introduction

Dye-sensitized solar cells (DSCs) belong to a class of modern photovoltaic technologies that have attracted widespread attention due to their potentially lower production costs and higher power conversion efficiencies.[1] In recent years, their overall performance has also been improved substantially by fine-tuning the morphology and hierarchical architecture of TiO_2 particles and photoanodes,[2] blocking charge recombination at the interface between TiO_2 and electrolytes, reducing the over-potential and increasing the rate of dye regeneration[3] and, finally, designing for more efficient and stable sensitizers.[4] Among all sensitizers, it is commonly accepted that Ru(II) complexes endowed with thiocyanate ligands have upheld a leading position in performance (e.g., conversion efficiency) issues among hundreds of dyes that have been scrutinized.[5] The studies on DSCs using functionalized derivatives of **N3** and **N749** are paradigms in this field, among which the champion efficiency using mesoporous TiO_2 layer and I^-/I_3^- redox couple under standard air mass 1.5 G sunlight stands presently at over 11%.[6]

Nonetheless, because of the possible dissociation of the thiocyanate ancillaries during device operation,[7] the use of the above mentioned **N3**, **N749**, and relevant Ru(II)-based sensitizers may only provide limited cell lifespans, and is thus considered as a major drawback of the current DSC embodiments. To further improve the stability of DSCs, development of Ru(II) sensitizers free of thiocyanate ancillaries is urgently demanded. One successful example should be ascribed to the employment of cyclometalating 4,6-difluorophenylpyridinato chelate for substitution of the two thiocyanate ligands from the **N3** coordination framework. The resulting sensitizer, bis(4,4′-dicarboxy-2,2′-bipyridine) 2-(2,4-difluorophenyl)pyridine ruthenium (II), coded as **YE05**, exhibits remarkable performance with short-circuit current density (J_{SC}) = 17 mA cm^{-2}, open-circuit voltage (V_{OC}) = 0.80 V, *FF* (fill factor) = 0.74, and efficiency $\eta = 10.1\%$.[8] In a similar fashion, van Koten,[9] Berlinguette,[10] and our team[11] have independently set out to explore the various viabilities of Ru(II) based polypyridine complexes with either tridentate or bidentate cyclometalating chelate as the DSC sensitizers.

In parallel to these literature precedents, we have gained more understanding from our previous research works that the pyrid-2-yl azolate (both pyrazolate and triazolate) chelate, due to their stronger electron deficient character,[12] can effectively

K.-L. Wu, W.-P. Ku, S.-W. Wang, Prof. Y. Chi
Department of Chemistry and Low Carbon Energy Research Center
National Tsing Hua University
Hsinchu 30013, Taiwan
E-mail: ychi@mx.nthu.edu.tw

K.-L. Wu, Dr. A. Yella, Dr. M. K. Nazeeruddin, Prof. M. Grätzel
Laboratory of Photonics and Interfaces
Institute of Chemical Sciences and Engineering
Ecole Polytechnique Fédérale de Lausanne (EPFL)
CH-1015 Lausanne, Switzerland
E-mail: mdkhaja.nazeeruddin@epfl.ch; michael.graetzel@epfl.ch

S.-H. Liu, Prof. P.-T. Chou
Department of Chemistry and Center for Emerging Material and Advanced Devices
National Taiwan University
Taipei 10617, Taiwan
E-mail: chop@ntu.edu.tw

DOI: 10.1002/adfm.201201876

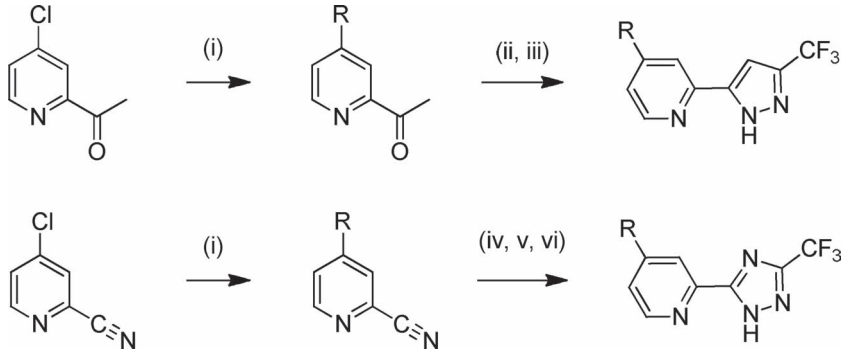

Scheme 1. Synthetic route to the functional pyrazole and triazole chelates; conditions: i) dioxaborolane, $Pd(PPh_3)_4$, K_2CO_3, reflux; ii) NaOEt, CF_3CO_2Et, THF; iii) N_2H_4, reflux; iv) NaOMe, EtOH, RT; v) NH_4Cl, reflux; vi) NaOH, trifluoroacetic acid hydrazide, reflux.

substitute the class of pyridinato cyclometalate in the assembly of potential high-efficiency Ru(II) sensitizers, for which their oxidation potential should be sufficiently more positive than that of I^-/I_3^- redox couple and, thus, the oxidized sensitizers can be easily regenerated back to the original state by electron donation from the redox couple in the electrolyte.[13] One representative sensitizer, coded **TFRS-2**, showed satisfactory cell performances with J_{SC} = 17.15 mA cm^{-2}, V_{OC} = 0.82 V, and FF = 0.678, corresponding to an overall conversion efficiency η = 9.54%.[14] In this contribution, we now report an extension by employing 4,4′-dicarbonylvinyl-2,2′-bipyridine as the TiO_2 anchor to demonstrate the ligand π-conjugation trait of these Ru(II) sensitizers, together with the studies of their intrinsic properties associated with the fine-tuning of pyrid-2-yl azolate chelates.

2. Results and Discussion

2.1. Synthesis and Characterization

The syntheses of 5-(pyrid-2-yl) pyrazole and 1,2,4-triazole chelates, together with a variety of thiophene appendages, are depicted in **Scheme 1**. The first step requires the preparation of the 4-chloro substituted 2-acetyl and 2-cyano pyridines that are not commercially available (see the Experimental Section for details). These pyridine compounds were treated with various dioxaborolane reagents under Suzuki cross-coupling conditions, allowing the addition of thiophene pendent at the 4-position of 2-acetyl and 2-cyano pyridine in moderate yields. The 2-acetyl or 2-cyano functional groups are then converted to pyrazole or triazole moieties using established cyclization protocols, among which the pyrazole is synthesized by initial Claisen condensation with ethyl trifluoroacetate, followed by treatment with hydrazine hydrate in refluxing ethanol,[15] while formation of triazole is best achieved by a prior ammonolysis of cyano group, followed by coupling with trifluoroacetic acid hydrazide at higher temperature.[16]

The 5-(pyrid-2-yl) azole ligands (i.e., either pyrazole or triazole) were reacted with the starting material [Ru{4,4′-bis(methoxycarbonylvinyl)-2,2′-bipyridine}(*p*-cymene)Cl]Cl to give the carbonylvinyl intermediates; the former is synthesized from addition of 4,4′-bis(methoxycarbonylvinyl)-2,2′-bipyridine to $[Ru(p\text{-cymene})Cl_2]_2$ using an approach described in the literature.[17] After chromatographic purification on a silica gel column to remove minor impurities, the obtained Ru(II) intermediates were hydrolyzed with aqueous NaOH in acetone to yield the Ru(II) sensitizers **TFRS-11–TFRS-14**. These Ru(II) complexes also represent a fraction of our current contribution aimed at designing efficient and robust, thiocyanate-free metal-based DSC sensitizers.[11,18]

In theory, addition of asymmetric chelate such as 5-(pyrid-2-yl) azole to the Ru(II) *p*-cymene intermediates is expected to afford up to three geometrical isomers if there involves limited or even no stereoselectivity. However, in certain cases, upon elongation of the reaction time and addition of alkali metal acetate as promoter the *trans*-di-azolate complexes were isolated as the dominant product. In accordance to this observation, the parent pyrid-2-yl azole chelate (fppzH), i.e., 2-(3-trifluoromethyl-1*H*-pyrazol-5-yl)pyridine, was known to react with $Ru_3(CO)_{12}$, affording the mononuclear Ru(II) complex $[Ru(fppz)_2(CO)_2]$ with *trans*-di-azolate, *cis*-di-pyridyl, and *cis*-di-carbonyl coordination configuration.[19] Thus, its stereoselectivity is also identical to that of the **TFRS-11–TFRS-14** sensitizers reported herein.

2.2. Optical Properties

The UV/Vis spectral data of these **TFRS** dyes in DMF are depicted in **Figure 1** and **Table 1**, together with those of **TFRS-2** as references for better understanding the systematic variation of the spectral pattern. As can be seen, all **TFRS-11–TFRS-14** complexes exhibit two lower lying absorption bands covering the visible region (400–700 nm), both of which are mainly

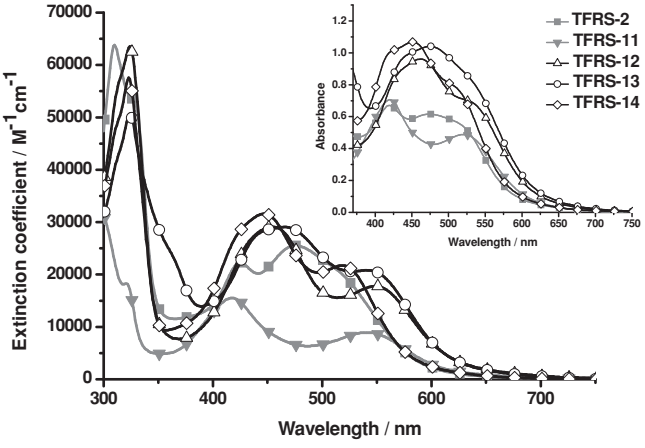

Figure 1. Absorption spectra of **TFRS-2** and **TFRS-11–TFRS-14** sensitizers in DMF. Inset: absorption spectra for all corresponding samples adsorbed on 6 μm of 20 nm TiO_2 thin film.

Table 1. Photophysical and electrochemical data of the studied **TFRS** sensitizers in DMF.

Dye	λ_{abs} [nm] (ε [L mol^{-1} cm^{-1}])[a)]	$E^{o\prime}{}_{ox}$[b)]	E_{0-0}[c)]	$E^{o\prime *}$[d)]
TFRS-11	321 (18 300), 419 (15 500), 545 (8 900)	0.83	1.74	−0.91
TFRS-12	324 (63 600), 456 (29 100), 551 (17 800)	0.81	1.74	−0.93
TFRS-13	324 (50 700), 467 (29 100), 543 (20 800)	0.81	1.79	−0.98
TFRS-14	323 (57 600), 448 (31 600), 521 (21 700)	1.03	1.88	−0.85
TFRS-2	310 (63 800), 426 (22 200), 477 (25 500), 516 (20 500)	0.90	1.91	−1.01

[a)]Absorption spectra were measured in DMF solution; [b)]Oxidation potential of dyes was measured in DMF with 0.1 M [TBA][PF_6] and with a scan rate of 50 mV s^{-1}; calibration was performed using Fc/Fc^+ as internal reference and converted to NHE by addition of 0.63 V; [c)]E_{0-0} was determined from the intersection of the absorption and tangent of the emission peak in DMF; [d)]$E^{o\prime *}$ was calculated as $E^{o\prime}{}_{ox} - E_{0-0}$.

attributed to the metal-to-ligand charge transfer (MLCT) transitions, mixed, to a certain extent, with the ligand-to-ligand π–π^* charge transfer transitions (LLCT). This assignment is firmly supported by computational approach (see the Supporting Information for details). As shown in Figures S1–S4 and Tables S1–S4 of the Supporting Information, the frontier analyses based on time-dependent DFT (TD-DFT) results suggest that the **TFRS** dyes share almost identical character for the lower electronic transitions, of which the optical excitation is mainly from the Ru(II) dπ orbital and occupied orbitals of pyrid-2-yl azolate chelates to the antibonding orbitals of the 4,4′-dicarboxyvinyl-2,2′-bipyridine chelate, denoted as MLCT and LLCT, respectively. Therefore, mixing of MLCT and $\pi\pi^*$ (LLCT) characters in the lower-lying transitions (greater than 420 nm) is unambiguous. Note that for all titled complexes the localized intra-ligand $\pi\pi^*$ transition (ILCT) appears with high oscillator strength in the region of 300–350 nm, corresponding to the S_9 and/or higher excited states, consistent with the experimental observation. For clarity, **Figure 2**a,b illustrate the calculated electronic transition and density plots for certain transitions of representative **TFRS-12** and **TFRS-14** sensitizers, respectively, in which the vertical bars are pertinent optical transitions with the oscillator strength of larger than 0.01. The suitability of this computational approach can be seen from the well fit of the major transition peaks to the absorption spectral profile in terms of position and intensity.

For a fair comparison, **TFRS-12**, a close analogue of **TFRS-2**, exhibits two lower-lying absorption bands at 456 ($\varepsilon \approx 29\,100$) and 551 nm ($\varepsilon \approx 17\,800$). Noticeably, these bands are more red-shifted and intense than those observed in **TFRS-2**, for which the relevant absorptions appeared at 426, 477, and 516 nm with slightly lower extinction coefficient of 22 200, 25 500 and 20 500 M^{-1} cm^{-1}, a result that is attributed to the reduced π-conjugation of 4,4′-dicarboxy-2,2′-bipyridine chelate in **TFRS-2**. Upon replacement of 5-hexylthiophen-2-yl in **TFRS-12** by 5-(hexylthio)thiophen-2-yl fragments, forming **TFRS-13** sensitizer (see **Scheme 2**), the MLCT/$\pi\pi^*$ signals became even more broadened and stronger in absorptivity, the result of which may be attributed to the sulfur atom having higher polarizability. This viewpoint is also supported by the computational approach, in which the maximum oscillator strength (greater than 450 nm, $f = 0.47$) for **TFRS-13** is greater than that (0.41) of **TFRS-12** (see Tables S2 and S3 of the Supporting Information). Alternatively, replacing pyrazolates of **TFRS-12** with the more electron-withdrawing triazolates, the sensitizer **TFRS-14** is expected to have stronger stabilization of the metal dπ orbitals, resulting in the lowering of the HOMO (highest occupied molecular orbital) energy level. However, such a lowering of energy is then counterbalanced with the decrease of the LUMO (lowest unoccupied molecular orbital) energy caused by the 4,4′-dicarboxyvinyl-2,2′-bipyridine anchor (c.f. 4,4′-dicarboxyl-2,2′-bipyridine in **TFRS-2**), such that **TFRS-14** showed comparable visible spectral coverage versus that of the **TFRS-2** sensitizer, except for the enhanced absorption cross section, i.e., the extinction coefficient. Finally, the vinyl linkage of the carboxyvinyl fragment is less efficient in terms of inducing both the bathochromic shift and hyperchromic effect versus that of the thiophen-2-yl group of the azolate ancillary. This delineation is confirmed by the less intense MLCT absorptions of **TFRS-11** versus those of **TFRS-2**. In fact, the computational results show smallest f strength of 0.28 (492 nm) among all titled complexes, consistent with the experimental UV/Vis spectra showed in Figure 1.

2.3. Electrochemical Studies

The electrochemical properties of these **TFRS** sensitizers were evaluated by cyclic voltammetry in DMF solution to give a preliminary assessment about the energetics of electron injection from the photoexcited sensitizers to the conduction band (CB) of TiO_2 and the subsequent regeneration of the oxidized sensitizers by the I^-/I_3^- redox couple. All potentials were measured in DMF solution with addition of 0.1 M [TBA][PF_6] and with a scan rate of 50 mV s^{-1}. The data was calibrated with Fc/Fc^+ internal reference and converted to value versus the normal hydrogen electrode (NHE) by addition of 0.63 V. As showed in Table 1, the Ru^{+2}/Ru^{+3} oxidation potentials ($E^{o\prime}{}_{ox}$) of **TFRS-11** to **TFRS-13** are within the narrow range 0.81–0.83 V (vs. NHE), which are more positive than that of I^-/I_3^- redox potential (approximately 0.35 V vs. NHE), but are slightly less positive than that of the **TFRS-2** reference sample (ca. 0.90 V vs. NHE) under identical condition.[20] The cathodic shift of oxidation potentials versus **TFRS-2** is apparently caused by the carboxyvinyl substituted bipyridine anchor, for which the greater π-conjugation is known to further destabilize the occupied frontier orbitals associated with this chelate. Among the titled Ru(II) complexes **TFRS-14** showed the greatest oxidation potential of 1.03 V, which is apparently caused by the influence of more electron-withdrawing triazolate groups. As these **TFRS** sensitizer exhibit more positive oxidation potential versus the I^-/I_3^- couple, they are subject to efficient regeneration by accepting electrons from surrounding iodide ions of electrolytic solution.

In a qualitative manner, the excited state oxidation potential ($E^{o\prime *}$) of sensitizers can be extracted from the aforementioned

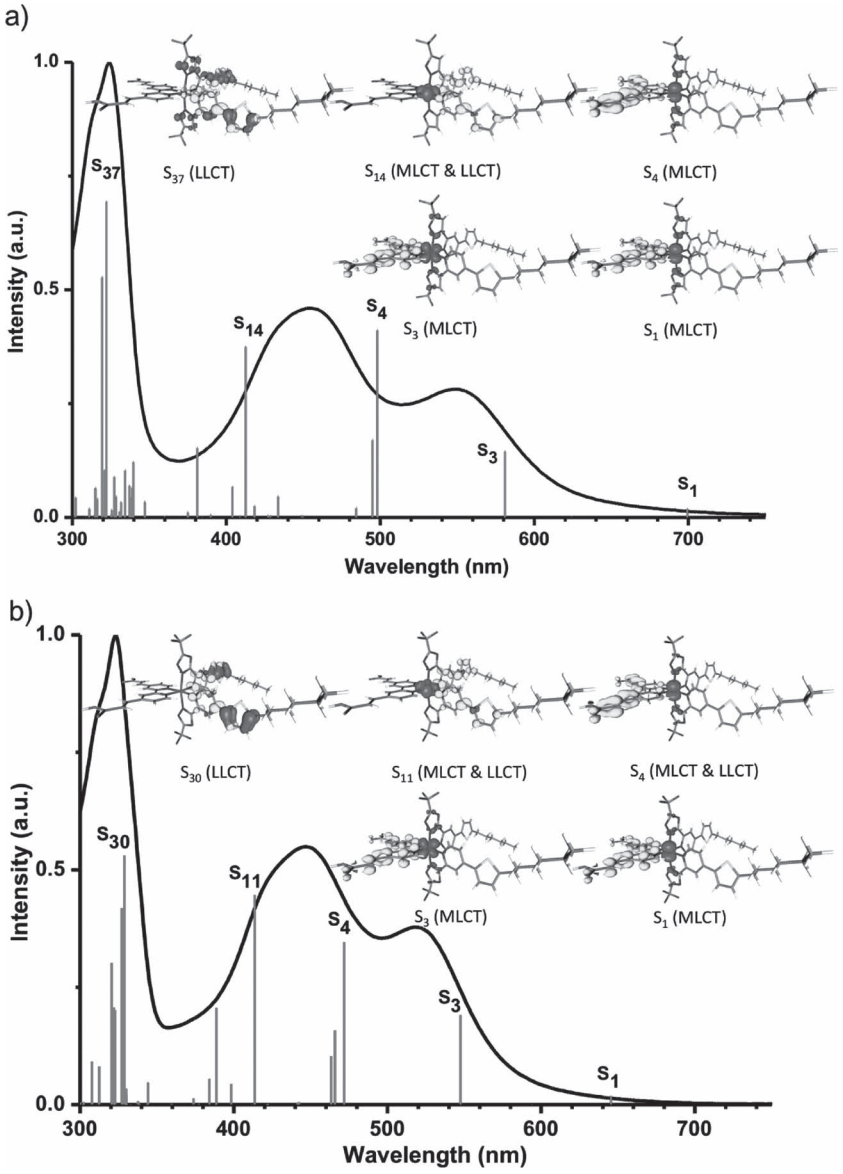

Figure 2. UV/Vis spectra and spin density plots for the specified transition of: a) **TFRS-12**, and, b) **TFRS-14**. The vertical bars are pertinent optical transitions with the oscillator strength of more than 0.01, for which occupied and unoccupied orbitals are represented in pink and yellow, respectively.

ground state oxidation potential ($E^{\circ\prime}_{ox}$) and the zero-zero-excited energy ($E_{0\text{-}0}$) according to the equation:

$$E^{\circ\prime *} = E^{\circ\prime}_{ox} - E_{0-0}$$

where $E_{0\text{-}0}$ was determined from the intersection of the absorption onset and tangent of the emission profile. It is believed that the $E^{\circ\prime *}$ value should be at least 0.2–0.3 V greater than the CB energy of TiO_2 photoanode to warrant favorable electron injection.[21] As can be seen in Table 1, the excited state oxidation potential ($E^{\circ\prime *}$) of these studied **TFRS** sensitizers fell in the range –0.85 to –0.98 V, which are all more negative than the CB edge of the TiO_2 anode (ca. –0.5 V vs. NHE) and hence guarantee the efficient injection of photoelectrons.

2.4. Photovoltaic Performance

DSCs were assessed by employing TiO_2 photoanodes with size 4 × 4 mm^2 and of two distinct thicknesses, namely 8 + 6 and 12 + 6 μm, consisting of mesoporous (20 nm) plus light-scattering (400 nm) layers. The double-layered architecture was employed to increase the light absorbing capability at the longer wavelength region.[22] The photoanodes were then stained in the respective dye solutions (0.3 mM) in ethanol, together with DMSO (20%, v/v) and CDCA (1 mM) for 18 h. An electrolyte solution consists of 0.6 M 1-methyl-3-propylimidazolium iodide (PMII), 0.03 M of iodine, 0.5 M 4-*tert*-butylpyridine (TBP), 0.1 M guanidinium thiocyanate, and 0.05 M LiI in a mixture of acetonitrile and valeronitrile (85:15, v/v). The cell performances were measured using a 6 × 6 mm^2 shadow mask to prevent excessive exposure to the simulated solar radiation.[23] As shown in **Table 2**, all of the carboxyvinyl-pyrazolate sensitizers, namely: **TFRS-11** to **TFRS-13**, showed higher J_{SC} and slightly lower V_{OC} upon using thicker TiO_2 photoanodes, yielding a better power conversion efficiency (η) compared to that of those fabricated using a thinner TiO_2 layer. The higher J_{SC} is attributed to the build-up of sufficient amount of dye molecules that adsorbed on the thicker TiO_2 layer, while the slightly lower V_{OC} is due to the increased surface area of the TiO_2 layer that provides additional charge recombination sites. The additional charge recombination sites are caused at the interface between TiO_2 and electrolyte, enhancing the dark current and

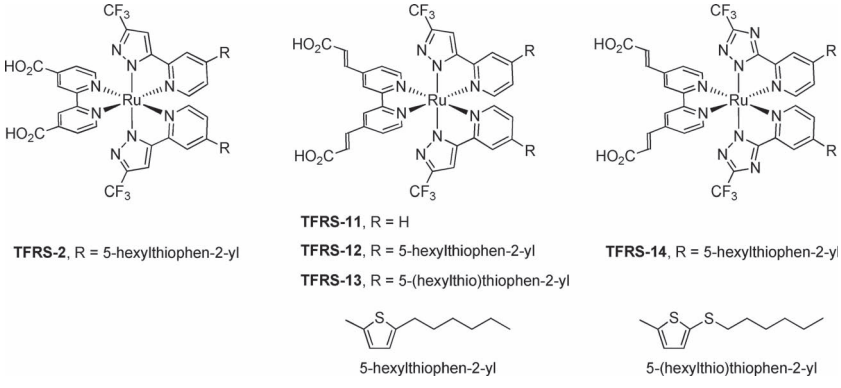

Scheme 2. Structural drawings of the Ru(II) sensitizers **TFRS-2** and **TFRS-11**–**TFRS-14**.

Table 2. The performances for DSCs measured under AM 1.5G one sun simulated irradiation.[a)]

Dye	TiO_2 [μm]	J_{SC} [mA cm^{-2}]	V_{OC} [V]	*FF*	η [%]	Dye loading[b)] [mol cm^{-2}]
TFRS-11	8 + 6	12.0	0.67	0.696	5.60	2.01×10^{-7}
	12 + 6	13.7	0.65	0.695	6.30	
TFRS-12	8 + 6	15.9	0.70	0.683	7.62	1.72×10^{-7}
	12 + 6	14.7	0.69	0.690	7.28	
TFRS-13	8 + 6	14.1	0.70	0.679	6.71	1.63×10^{-7}
	12 + 6	14.7	0.67	0.664	6.68	
TFRS-14	8 + 6	15.2	0.78	0.713	8.44	1.67×10^{-7}
	12 + 6	16.4	0.77	0.698	9.02	
TFRS-2	8 + 6	14.9	0.78	0.690	8.29	1.62×10^{-7}
	12 + 6	19.4	0.75	0.661	9.82	

[a)]All devices were fabricated using double-layered TiO_2 anode and with 4×4 mm^2 working area, an electrolyte that consists of 0.6 M PMII, 0.03 M I_2, 0.5 M TBP, 0.1 M GNCS, and 0.05 M LiI in the mixed valeronitrile/acetonitrile solution (15:85, v/v); also, all as - prepared devices were covered by a 6×6 mm^2 shadow mask for the performance measurement; [b)]The dye loading on 12 + 6 μm TiO_2 films was conducted by desorbing the dye into 0.1 M tetrabutylammonium hydroxide solution in MeOH and H_2O (volume ratio: 1:1) and then measured using the UV/Vis spectral analysis.

lowering the photovoltage.[24] The only exception is **TFRS-12**, for which the efficiency (η) of 8 + 6 μm cell is recorded to be 7.62%, which is slightly higher than that of η = 7.28% obtained for the 12 + 6 μm cell, a result of the higher J_{SC} of 15.9 mA cm^{-2}. This observation implies that the **TFRS-12** sensitizer, with 5-hexylthiophen-2-yl pendants, has the best light harvesting ability among the carboxyvinyl-pyrazolate sensitizers. Furthermore, the small decrease in the cell performances for **TFRS-13** versus **TFRS-12** may be attributed to the slightly stronger binding of its 5-hexythiothiophen-2-yl group with I_3^- ions in electrolyte, which then increased its local concentration near the TiO_2 surface and, concurrently, the rate of electron recombination.[25]

Under identical conditions, the **TFRS-2** reference sensitizer displays J_{SC} of 14.9 and 19.4 mA cm^{-2}, V_{OC} of 0.78 and 0.75 V, and overall power conversion efficiency of 8.29% and 9.82% for DSCs that employed 8 + 6 μm and 12 + 6 μm of TiO_2 photoanode, respectively. These performance characteristics represent the best data ever recorded for this class of sensitizers and are superior to those of **TFRS-12**, which is a close analogue to **TFRS-2** that differs only by the carboxyvinyl anchor. Thus, despite the increase of dye loading (see Table 2) and more intense absorptivity, **TFRS-12** is still not able to boost the DSCs' efficiencies (cf. **TFRS-2**). On the one hand, this inferior performance could be a result of less efficient blocking of the TiO_2 surface due to the increased spatial separation from the Ru(II) core framework,[26] which allows the I_3^- anion to penetrate into the TiO_2/sensitizer interface, resulting in a faster charge recombination. On the other hand, the less positive ground-state oxidation potential of **TFRS-12** ($E^{o\prime}_{ox}$ = 0.81 V vs. NHE) would also reduce the thermodynamic driving force for the dye regeneration by I^- ions, giving relatively poor device performances. In fact, all of the carboxyvinyl-pyrazolate sensitizers **TFRS-11** to **TFRS-13** showed potentials that are smaller than that of $I^-/I_2^{\bullet-}$ couple (ca. 0.79 ± 0.1 V vs. NHE)),[27] implying the occurrence of inefficient dye regeneration. In contrast, the pristine Ru(II)-based sensitizers **N3** and **Z907** and their carboxyvinyl analogues, coded **K8** and **K9**, all showed relatively more positive ground state oxidation potential at the vicinity of 0.9 V versus NHE.[28] Even the recently reported amphiphilic Ru(II) complex **BTC-2**, in which the bipyridine anchor is incorporated with the unique 5-carboxythiophen-2-yl units, has shown a slightly more positive oxidation potential of 0.84 V versus NHE.[29] As a result, the driving force for dye regeneration is expected to be more efficient. Thus, as the V_{OC} turned smaller for DSCs with **K8**, **K9**, and **BTC-2**, their increased absorption extinction coefficient of the carboxyl anchor enables notable enhancement in J_{SC} versus the DSCs fabricated with **N3** and **Z907**. The net result gives a better performance, particularly for those fabricated with thinner TiO_2 layer. In good agreement with this finding, the carboxyvinyl-triazolate sensitizer **TFRS-14** exhibits the most positive oxidation potential $E^{o\prime}_{ox}$ of 1.03 V (see Table 2) due to the reduced electron density at the Ru(II) metal center that exerted by the better electron accepting triazolate moieties. The increase of dye regeneration efficiency (from electrolyte) then makes this triazolate sensitizer **TFRS-14** superior in DSCs performance versus all carboxyvinyl-pyrazolate sensitizers **TFRS-11** to **TFRS-13** elaborated in this study.

The *J–V* characteristics and incident photon-to-current conversion efficiency (IPCE) action diagrams are depicted in **Figure 3**. It is notable that **TFRS-2**, which possesses the parent 4,4′-dicarboxy-2,2′-bipyridine anchor, exhibits the best *J–V* characteristics and IPCE at all wavelengths among these series of Ru(II) sensitizers, c.f. **TFRS-11** to **TFRS-14**. On the other hand, the IPCE of the second-best sensitizer **TFRS-14** only maintains a plateau of over 70% from 420 to 570 nm, with a maximum of ca. 77% at ca. 510 nm, which is about 7% lower than that of **TFRS-2** at the same position, showing inferior light-harvesting efficiency. Moreover, the *J–V* characteristics and the IPCE data of **TFRS-11** to **TFRS-13** are all inferior than **TFRS-14**; the origin of this can be traced back to the previous discussion.

To gain more insight into the intrinsic DSCs property, electrochemical impedance spectroscopy was performed to analyze

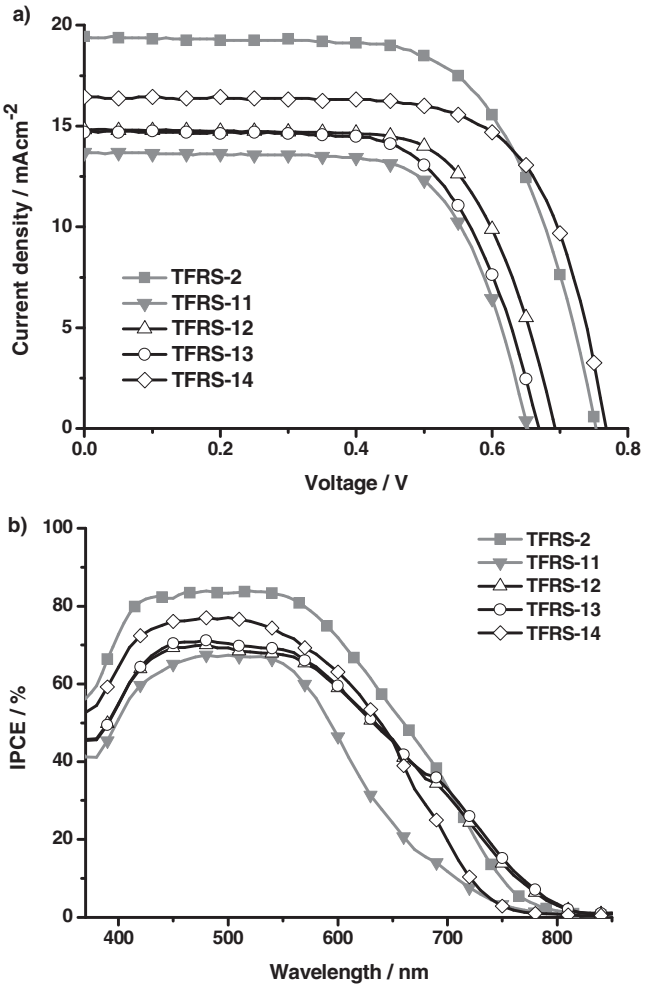

Figure 3. a) *J–V* characteristics and b) IPCE spectra for DSCs with 12 + 6 µm TiO_2 layer and measured under AM 1.5G simulated solar irradiation.

Transient photocurrent and photovoltage decay measurements were carried out in order to investigate the rates of interfacial recombination of electrons from the TiO_2 conduction band to electrolyte. The density of state (DOS) of the films loaded with sensitizer was determined from transient photocurrent decay measurements. The chemical capacitance $C\mu$ for the **TFRS** sensitizer films as a function of V_{OC} are compiled in **Figure 5**a. $C\mu$ is directly proportional to the DOS: $C\mu = q(e)$DOS, where $q(e)$ is the charge of one electron. The $C\mu$ values are very similar for the **TFRS** sensitizers, with small differences being noted only at $V_{OC} > 0.6$ V. This observation rules out any substantial contribution of a conduction band shift to the observed decrease in the back-electron transfer rate. Figure 5b illustrates electron lifetime as a function of V_{OC} for the different sensitizers. The V_{OC} was adjusted by varying the intensity of the bias light impinging on the cell. The trend correlates rather well with the V_{OC} values obtained for these devices, i.e., as electron lifetime gets shorter, V_{OC} decreases. Longer electron lifetimes were observed for **TFRS-12**, compared to the **TFRS-13**. This difference in charge separation lifetime can be explained by various degrees of electrolyte/dye interactions. Several authors have reported previously that atoms such as sulfur and oxygen can bind I_3^- and I_2 species, forming charge-transfer complexes. This can lead to a higher concentration of these species at TiO_2 surface, catalyzing e^-_{TiO2}/electrolyte recombination.[30] Therefore, **TFRS-13**, which contains one additional sulfur atom compared to **TFRS-12**, would be expected to bind I_3^- and I_2 species leading to faster recombination.

In view of the long-term stability, a high-performance electrolyte based on butyronitrile (BN) was selected.[31] Initially, the fabricated devices showed maximum performance characteristics of J_{SC} = 18.3 mA cm^{-2}, V_{OC} = 0.70 V, FF = 0.637 and η = 8.16% for **TFRS-2** and of 15.8 mA cm^{-2}, 0.70 V, 0.686 and 7.59% for **TFRS-14** at 200 h (**Figure 6**). After 1000 h of light soaking at 60 °C, the device parameters of **TFRS-2** vary only slightly from the initial values, affording J_{SC} = 17.3 mA cm^{-2}, V_{OC} = 0.70 mV, FF = 0.621 and η = 7.52% at the end of the

the effects on charge generation, transport, and collection. **Figure 4** depicts the impedance spectra of DSCs fabricated with **TFRS-11** to **TFRS-14** sensitizers and **TFRS-2** reference, in the dark under a forward bias of 0.65 V. As a result, the radius of these semicircles revealed a descending order of **TFRS-14** (342.7 Ω) > **TFRS-2** (225.7 Ω) > **TFRS-13** (109.9 Ω) > **TFRS-11** (78.6 Ω) ≈ **TFRS-12** (77.2 Ω), indicating that the recombination process from the as prepared **TFRS-14** cell is the slowest of all, including that of **TFRS-2**, leading to the highest photovoltage. On the other hand, all other sensitizers **TFRS-11** to **TFRS-13** showed much inferior performance compared to that of **TFRS-2** standard that without the carboxyvinyl groups. The results are also consistent with the measured V_{OC} values listed in Table 2.

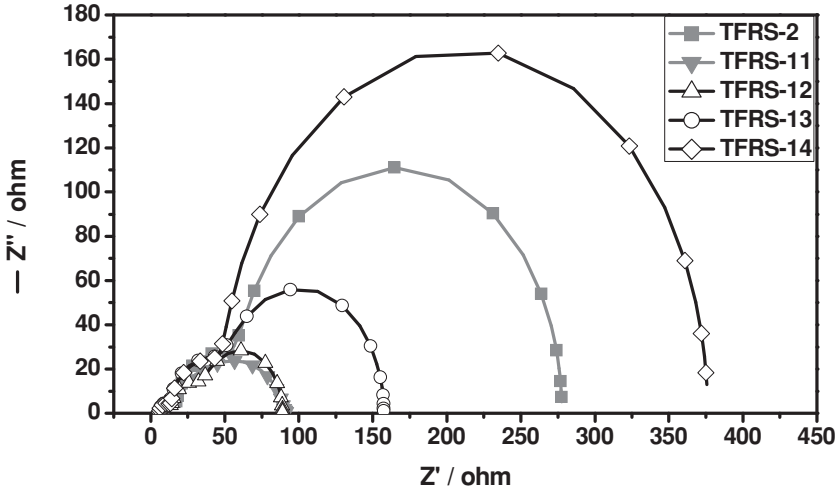

Figure 4. Electrochemical impedance spectra measured under dark at a forward bias of 0.65 V for the cells employing different **TFRS** dyes.

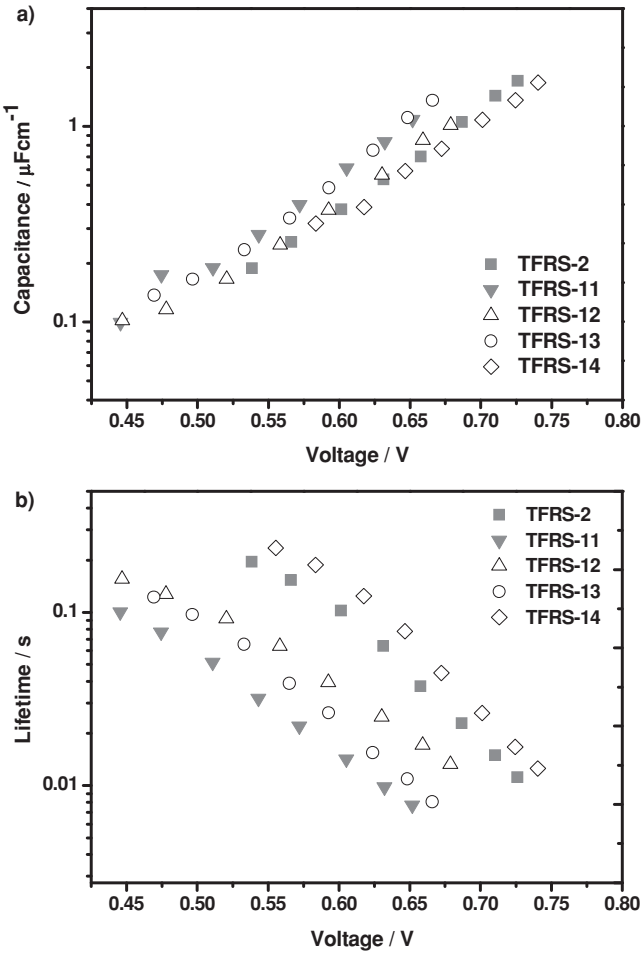

Figure 5. Electron capacitance (a) and lifetime (b) determined with photocurrent and photovoltage decay measurements of devices with **TFRS** dyes.

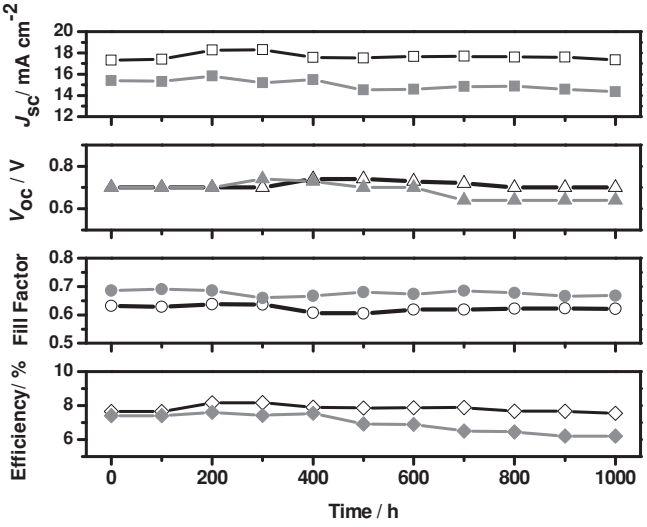

Figure 6. Evolution of solar cell parameters of **TFRS-2** (open squares) and **TFRS-14** (closed squares) measured under the irradiance of AM 1.5 G sunlight-soaking at 60 °C. A 370 nm cut-off long pass filter was put on the cell surface during illumination. Electrolyte: 1.0 M DMII, 0.15 M iodine, 0.1 M GNCS, 0.1 M LiI, and 0.5 M NBB (*N*-butyl-1*H*-benzimidazole) in butyronitrile.

experiment. As the result, the overall efficiency retained 92% of its initial value, confirming its excellent stability. On the other hand, the photovoltaic performance of the carboxyvinyl sensitizer **TFRS-14** suffers a much severe decline from the initial values, giving J_{SC} = 14.4 mA cm^{-2}, V_{OC} = 0.64 mV, FF = 0.668 and η = 6.16%, and afforded total reduction of overall efficiency by 18% after 1000 hours of light soaking. Since none of these sensitizers possess the thiocyanate ancillary, the instability is most probably caused by the carboxyvinyl anchors that existed in the **TFRS-14** sensitizer.

3. Conclusions

In summary, we have reported a new series of *tris*-bidentate Ru(II) sensitizers (**TFRS-11** to **TFRS-14**), in which a pair of carboxyvinyl fragments are strategically added to replace the carboxyl group of typical 4,4′-dicarboxy-2,2′-bipyridine anchor. These new carboxyvinyl anchors would increase the light-harvesting as confirmed by their absorption spectra and verified using DFT calculations. However, due to the concomitant reduction of their ground state oxidation potentials, of 0.81–0.83 V vs. NHE, caused by increasing π-conjugation, the best DSC devices among the pyrazolate sensitizers **TFRS-11** to **TFRS-13** afforded an overall conversion efficiency of 7.62%, which is obtained by **TFRS-12** and is still lower than that of the reference **TFRS-2** that possesses only typical carboxyl anchors. The poor match in oxidation potential versus that of I^-/I_3^- couple can be corrected using the carboxyvinyl-triazolate **TFRS-14**, for which the more positive $E^{\circ\prime}_{ox}$ of 1.03 V improves the dye regeneration efficiency and showing performances superior to all other carboxyvinyl sensitizers elaborated in this study.

Finally, as showed by the light soaking experiments conducted at 60 °C for 1000 hours, the **TFRS-14** device showed higher degradation versus those of the **TFRS-2** reference cell. Such an observation may reflect the higher reactivity between C=C double bond (vinyl group) and halogen element (both I^- and I_3^-) present in the electrolytes. Clearly, such a structural modification should be avoided in future designs.

4. Experimental Section

General Procedures: All reactions were performed under argon atmosphere and solvents were distilled from appropriate drying agents prior to use. Commercially available reagents were used without further purification unless otherwise stated. 4,4′-Bis(methoxycarbonylvinyl)-2,2′-bipyridine and the corresponding Ru(II) complex [Ru{4,4′-bis(methoxycarbonylvinyl)-2,2′-bipyridine}(*p*-cymene)Cl]Cl were synthesized according to the literature procedures.[28a,32] 2-Acetyl-4-chloropyridine was prepared from a two-step process involving combination of picolinic acid, NaBr, and thionyl chloride to afford first 4-chloro-2-methoxycarbonylpyridine;[33] next, it was converted to the desired acetyl compound by sequential Claisen condensation and decarboxylation,[34] while the respective 2-cyano-4-chloro-pyridine was obtained in high yield from treatment of 4-cholropyridine *N*-oxide with dimethylcarbamyl chloride and trimethylsilanecarbonitrile.[35] All

reactions were monitored using pre-coated TLC plates (0.20 mm with fluorescent indicator UV254). Mass spectra were obtained on a JEOL SX-102A instrument operating in electron impact (EI) or fast atom bombardment (FAB) mode. ^{1}H spectra were recorded on a Varian Mercury-400 instrument. Elemental analysis was carried out with a Heraeus CHN-O Rapid Elementary Analyzer.

Synthesis of ***TFRS-11***: 2-(3-(Trifluoromethyl)-1*H*-pyrazol-5-yl) pyridine (90.0 mg, 0.422 mmol), [Ru{4,4′-bis(methoxycarbonylvinyl)-2,2′-bipyridine}(*p*-cymene)Cl]Cl (125 mg, 0.211 mmol) and potassium acetate (206 mg, 2.11 mmol) were dissolved in xylenes (20 mL). The mixture was refluxed for 5 h. After removing the solvent, the residue was extracted with CH_2Cl_2 (3 × 25 mL), washed with water and concentrated to dryness. The mixture of products was purified by silica gel column chromatography (CH_3CN/CH_2Cl_2 = 1:5). Next, the solid product was dissolved in a mixture of acetone (20 mL) and 1 M NaOH solution (1.2 mL). The solution was heated to 60 °C under nitrogen for 2 h. After then, the solvent was removed under vacuum and the residue was dissolved in 10 mL of H_2O. The solution was titrated with 2 M HCl to pH 3 to afford a dark brown precipitate. The dark brown precipitate was washed with deionized water, acetone and diethyl ether in sequence, giving dark brown solid (47.0 mg, 28%).

Spectral Data of ***TFRS-11***: MS (FAB, ^{102}Ru): *m/z* 822 $(M)^+$. ^{1}H NMR (400 MHz, d_6-DMSO, 298 K): δ 9.05 (s, 2H), 8.19 (d, J = 7.6 Hz, 2H), 7.94 (t, J = 8.2 Hz, 2H), 7.81 (d, J = 4.8 Hz, 2H), 7.71–7.47 (m, 6H), 7.38–7.25 (m, 4H), 7.05 (d, J = 16 Hz, 2H). ^{19}F NMR (376 MHz, d_6-DMSO, 298K): δ –58.00 (s, 6F). Anal. Calcd. for $C_{34}H_{22}F_6N_8O_4Ru{\cdot}H_2O$: C, 48.63; N, 13.35; H, 2.88; found: C, 48.70; N, 13.06; H, 3.33.

Synthesis of ***TFRS-12***, ***TFRS-13***, *and* ***TFRS-14***: A similar procedure was used as described for **TFRS-11**, employing 4-(5-hexylthiophen-2-yl)-2-(3-trifluoromethyl-1*H*-pyrazol-5-yl)pyridine (144 mg, 0.380 mmol, and respective Ru(II) source reagent. The residue was purified by silica gel column chromatography (ethyl acetate/CH_2Cl_2 = 1:10). After hydrolysis, the sensitizer ***TFRS-12*** was obtained as a greenish-brown solid (69.6 mg, 31%). Other derivatives, namely: ***TFRS-13*** and ***TFRS-14***, were synthesized in approx. 25% yield using 4-(5-(hexylthio)thiophen-2-yl)-2-(3-trifluoromethyl-1*H*-pyrazol-5-yl)pyridine and 4-(5-hexylthiophen-2-yl)-2-(3-trifluoromethyl-1*H*-1,2,4-triazol-5-yl)pyridine as the starting material.

Spectral Data of ***TFRS-12****:* MS (FAB, ^{102}Ru): *m/z* 1155 $(M+1)^+$. ^{1}H NMR (400 MHz, d_6-DMSO, 298 K): δ 9.08 (s, 2H), 8.53 (s, 2H), 8.02–7.88 (m, 4H), 7.82 (d, J = 3.4 Hz, 2H), 7.71–7.56 (m, 4H), 7.50 (d, J = 5.6 Hz, 2H), 7.24 (s, 2H), 7.06 (d, J = 16 Hz, 2H), 6.96 (d, J = 3.4 Hz, 2H), 2.81 (t, J = 7.4 Hz, 4H), 1.66–1.54 (m, 4H), 1.35–1.16 (m, 12H), 0.81 (t, J = 6.4 Hz, 6H). ^{19}F NMR (376 MHz, d_6-DMSO, 298K): δ –58.00 (s, 6F). Anal. Calcd. for $C_{54}H_{50}F_6N_8O_4RuS_2{\cdot}5H_2O$: C, 52.12; N, 9.01; H, 4.80; found: C, 51.82; N, 8.93; H, 4.51.

Spectral Data of **TFRS-13***:* MS (FAB, ^{102}Ru): *m/z* 1219 $(M+1)^+$. ^{1}H NMR (400 MHz, d_6-DMSO, 298K): δ 9.01 (s, 2H), 8.24 (s, 2H), 8.02 (d, J = 6.0 Hz, 2H), 7.81 (d, J = 3.6 Hz, 2H), 7.69–7.53 (m, 4H), 7.50–7.39 (m, 4H), 7.24 (d, J = 3.6 Hz, 2H), 7.09 (d, J = 4.8 Hz, 2H), 7.01 (d, J = 16 Hz, 2H), 2.91 (t, J = 7.0 Hz, 4H), 1.63–1.50 (m, 4H), 1.42–1.20 (m, 12H), 0.82 (t, J = 6.6 Hz, 6H). ^{19}F NMR (376 MHz, d_6-DMSO, 298K): δ –58.21 (s, 6F). Anal. Calcd. for $C_{54}H_{50}F_6N_8O_4RuS_4{\cdot}2H_2O$: C, 51.74; N, 8.93; H, 4.34; found: C, 51.65; N, 8.82; H, 4.27.

Spectral Data of **TFRS-14**: MS (FAB, ^{102}Ru): *m/z* 1157 $(M+1)^+$. ^{1}H NMR (400 MHz, d_6-DMSO, 298 K): δ 9.03 (s, 2H), 8.17 (s, 2H), 8.01 (d, J = 5.6 Hz, 2H), 7.81 (d, J = 3.6 Hz, 2H), 7.70–7.55 (m, 6H), 7.27 (d, J = 6.0 Hz, 2H), 7.02 (d, J = 16 Hz, 2H), 6.96 (d, J = 3.2 Hz, 2H), 2.82 (t, J = 7.2 Hz, 4H), 1.68–1.55 (m, 4H), 1.36–1.18 (m, 12H), 0.83 (t, J = 6.4 Hz, 6H). ^{19}F NMR (376 MHz, d_6-DMSO, 298K): δ –61.77 (s, 6F). Anal. Calcd. for $C_{52}H_{48}F_6N_{10}O_4RuS_2{\cdot}H_2O$: C, 53.19; N, 11.93; H, 4.29; found: C, 52.87; N, 12.10; H, 4.75.

DFT Calculations: All calculations on were performed with the Gaussian 09 program package.[36] Their ground state structures were first optimized with density functional theory (DFT) at B3LYP/LANL2DZ (Ru) and 6-31G* (H, C, N, O, F, S) level. The optimized structures were then used to calculate 60 lowest singlet energy optical excitations using the time-dependent density functional theory (TD-DFT) method. To mimic the realistic environmental perturbation, a polarizable continuum model (PCM) was applied using dimethylformamide (DMF) as solvent.

Device Fabrication: The fluorine-doped tin oxide (FTO) glass (3.2 mm thickness, sheet resistance of 9 Ω cm^{-2}, Pilkington) was first cleaned in a detergent solution using an ultrasonic bath for 30 min, and then rinsed with water and ethanol in sequence. After treated with ozone generated from PSD series UV-ozone cleaning system for 15 min (Novascan Technologies, Inc.), the FTO glasses were immersed into a 40 mM aqueous $TiCl_4$ solution at 70 °C for 30 min and washed with water and ethanol. The photoanodes composed of nanocrystalline TiO_2 were prepared using a previously reported procedure. The TiO_2 electrodes of 12 μm thickness were deposited on transparent conducting glass, over which a scattering layer of 6 μm thickness containing 400 nm TiO_2 particles (PST-400, JGC Catalysts and Chemicals, Japan) was screen-printed (active area, 0.16 cm^2). TiO_2 film thickness was measured by alpha-step IQ surface profile (KLA Tencor). The TiO_2 electrodes were heated under an air flow at 325 °C for 30 min, followed by heating at 375 °C for 5 min, 450 °C for 15 min, and 500 °C for 15 min. The TiO_2 electrodes were treated with a 40 mM aqueous solution of $TiCl_4$, sintered at 70 °C for 30 min and then washed with water and ethanol. The electrodes were heated again at 500 °C for 30 min and left to cool to 80 °C before dipping into the dye solution (0.3 mM) containing 20% DMSO in ethanol for 18 h at 25 °C. The Pt counter electrodes were next prepared by spin-coating employing an H_2PtCl_6 solution (2 mg of Pt in 1 mL isopropyl alcohol) on FTO plates, followed by sintering at 400 °C for 15 min. The dye-sensitized TiO_2 electrodes were assembled with Pt counter electrodes by heating with a hot-melt Surlyn film (Meltonix 1170-25, 25 μm, Solaronix) as spacer between the electrodes, and then heated at 130 °C. The electrolyte containing 0.6 M 1-methyl-3-propylimidazolium iodide (PMII), 0.03 M of iodine, 0.5 M *tert*-butylpyridine (TBP), 0.1 M guanidinium thiocyanate, and 0.05 M of LiI in the mixed valeronitrile/acetonitrile solution with volume ratio of 15:85, which was then injected into the cell through a drilled hole at the counter electrode. Finally, the hole was sealed using a hot-melt Surlyn film and a cover glass. In order to reduce scattered light from the edge of glass electrodes, a light-shading mask (0.36 cm^2) was used to cover the device assembly. The dye loading on 12 + 6 μm TiO_2 films was measured by desorbing the dye into a 0.5 M tetrabutylammonium hydroxide solution in MeOH and H_2O mixture (volume ratio: 1:1), followed by detecting their absorbance using the UV/Vis spectrometer.

Photovoltaic Characterization: Photovoltaic measurements were recorded with a Newport Oriel Class A Solar Simulator (Model 91159) equipped with a class A 150 W xenon light source powered by a Newport power supply (Model 69907). The light output (area: 2 × 2 in.) was calibrated to AM 1.5 using a Newport Oriel correction filter to reduce the spectra mismatch in the region of 350–750 nm to less than 4%. The power output of the lamp was calibrated to 1 Sun (100 mWcm^{-2}) using a certified Si reference cell (SRC-1000-TC-QZ, VLSI standard S/N: 10510-0031). The current voltage characteristic of each cell was obtained by applying an external potential bias to the cell and measuring the generated photocurrent with a Keithley digital source meter (Model 2400). The spectra of incident photon-to-current conversion efficiency (IPCE) were calculated with the equation $1240J_{SC}(\lambda)/(\lambda P_{in}(\lambda))$, where J_{SC} is the short-circuit current density under each monochromatic illumination in A cm^{-2}, λ is the wavelength of incident monochromatic light in nm, and P_{in} is the monochromatic light intensity in W cm^{-2}, and plotted as a function of incident wavelength with increments of 10 nm. It should be noted that 20 values of J_{SC} (interval 50 ms) were collected after a device was illuminated monochromatically 3 s later and were averaged for calculation of IPCE.[37] A 300 W Xe lamp (Model 6258, Newport Oriel) combined with an Oriel cornerstone 260 1/4 m monochromator (Model 74100) provided an unchopped monochromatic beam onto a photovoltaic cell. The beam intensity was calibrated with a power meter (Model 1936-C, Newport) equipped with a Newport 818-UV photodetector.

Electrical Impedance Measurements: Electrical impedance experiments were carried out with a PARSTAT 2273 (AMETEK Princeton Applied Research, U.S.A.) electrochemical workstation, with a frequency range of 0.05–10^6 Hz and a potential modulation of 5 mV.

Transient Photocurrent/ Photovoltage Measurements: Transient decays were measured under a varying white-light bias with superimposed red-light perturbation pulses (both light sources were light-emitting diodes (LEDs)). The voltage dynamics were recorded by using a Keithley 2400 source meter. Varying the intensity of white-light bias allowed the estimate of recombination rate constant (and thus apparent electron lifetime) at different open-circuit potentials by controlling the concentration of the free charges in TiO_2. Red perturbation pulses were controlled not to exceed 5% of the signal resulting from the white bias (either current or voltage) in order to maintain single-exponential voltage decay.

Stability Test: The photoanodes of the device employed in this study are composed of a 12 μm transparent TiO_2 thin film and a 6 μm thick layer of 400 nm TiO_2 particles. A 370 nm cut-off long pass filter film was attached on the cell surface during illumination. The cell was irradiated under a Suntest CPS plus lamp (ATLAS GmbH, 100 mW cm^{-2}) during visible-light soaking at 60 °C. The electrolyte consisted of 1.0 M DMII, 0.15 M iodine, 0.1 M GNCS, 0.1 M LiI, and 0.5 M NBB (*N*-butyl-1*H*-benzimidazole) in butyronitrile (BN).

Supporting Information

Supporting Information is available from the Wiley Online Library or from the author.

Acknowledgements

K.-L.W. and W.-P.K. contributed equally to this work. Y.C. thanks the National Science Council of Taiwan (NSC-101-3113-E-007-006) for financial support. K.-L.W. is a recipient of the Graduate Students Study Abroad Program sponsored by National Science Council of Taiwan. A.Y. thanks the Balzan foundation for financial support under the Balzan Prize 2009 awarded to M.G.

Received: July 6, 2012
Revised: September 9, 2012
Published online: December 10, 2012

[1] a) M. Grätzel, *Acc. Chem. Res.* **2009**, *42*, 1788; b) L. M. Goncalves, V. de Zea Bermudez, H. A. Ribeiro, A. M. Mendes, *Energy Environ. Sci.* **2008**, *1*, 655; c) N. Armaroli, V. Balzani, *Angew. Chem. Int. Ed.* **2007**, *46*, 52; d) J. R. Durrant, S. A. Haque, E. Palomares, *Chem. Commun.* **2006**, 3279.

[2] a) Y. J. Kim, M. H. Lee, H. J. Kim, G. Lim, Y. S. Choi, N.-G. Park, K. Kim, W. I. Lee, *Adv. Mater.* **2009**, *21*, 3668; b) X. Wu, Z. Chen, G. Q. Lu, L. Wang, *Adv. Funct. Mater.* **2011**, *21*, 4167; c) F. Sauvage, D. Chen, P. Comte, F. Huang, L.-P. Heiniger, Y.-B. Cheng, R. A. Caruso, M. Grätzel, *ACS Nano* **2010**, *4*, 4420.

[3] a) S. Yanagida, Y. Yu, K. Manseki, *Acc. Chem. Res.* **2009**, *42*, 1827; b) T. W. Hamann, R. A. Jensen, A. B. F. Martinson, H. Van Ryswyk, J. T. Hupp, *Energy Environ. Sci.* **2008**, *1*, 66.

[4] a) H. Imahori, T. Umeyama, S. Ito, *Acc. Chem. Res.* **2009**, *42*, 1809; b) A. Reynal, E. Palomares, *Eur. J. Inorg. Chem.* **2011**, 4509; c) Y. Ooyama, Y. Harima, *Eur. J. Org. Chem.* **2009**, 2903; d) G. C. Vougioukalakis, A. I. Philippopoulos, T. Stergiopoulos, P. Falaras, *Coord. Chem. Rev.* **2011**, *255*, 2602; e) A. Yella, H.-W. Lee, H. N. Tsao, C. Yi, A. K. Chandiran, M. K. Nazeeruddin, E. W.-G. Diau, C.-Y. Yeh, S. M. Zakeeruddin, M. Grätzel, *Science* **2011**, *334*, 629.

[5] a) P. Wang, S. M. Zakeeruddin, J. E. Moser, M. K. Nazeeruddin, T. Sekiguchi, M. Grätzel, *Nat. Mater.* **2003**, *2*, 402; b) C.-Y. Chen, M. Wang, J.-Y. Li, N. Pootrakulchote, L. Alibabaei, C.-H. Ngoc-Le, J.-D. Decoppet, J.-H. Tsai, C. Grätzel, C.-G. Wu, S. M. Zakeeruddin, M. Grätzel, *ACS Nano* **2009**, *3*, 3103; c) Y. Cao, Y. Bai, Q. Yu, Y. Cheng, S. Liu, D. Shi, F. Gao, P. Wang, *J. Phys. Chem. C* **2009**, *113*, 6290; d) S.-H. Yang, K.-L. Wu, Y. Chi, Y.-M. Cheng, P.-T. Chou, *Angew. Chem. Int. Ed.* **2011**, *50*, 8270; e) Y.-S. Yen, H.-H. Chou, Y.-C. Chen, C.-Y. Hsu, J. T. Lin, *J. Mater. Chem.* **2012**, *22*, 8734; f) H.-W. Lin, Y.-S. Wang, Z.-Y. Huang, Y.-M. Lin, C.-W. Chen, S.-H. Yang, K.-L. Wu, Y. Chi, S.-H. Liu, P.-T. Chou, *Phys. Chem. Chem. Phys.* **2012**, *14*, 14190.

[6] a) M. Grätzel, *Inorg. Chem.* **2005**, *44*, 6841; b) L. Han, A. Islam, H. Chen, C. Malapaka, B. Chiranjeevi, S. Zhang, X. Yang, M. Yanagida, *Energy Environ. Sci.* **2012**, *5*, 6057.

[7] F. Nour-Mohhamadi, S. D. Nguyen, G. Boschloo, A. Hagfeldt, T. Lund, *J. Phys. Chem. B* **2005**, *109*, 22413.

[8] T. Bessho, E. Yoneda, J.-H. Yum, M. Guglielmi, I. Tavernelli, H. Imai, U. Rothlisberger, M. K. Nazeeruddin, M. Grätzel, *J. Am. Chem. Soc.* **2009**, *131*, 5930.

[9] a) S. H. Wadman, J. M. Kroon, K. Bakker, M. Lutz, A. L. Spek, G. P. M. van Klink, G. van Koten, *Chem. Commun.* **2007**, 1907; b) S. H. Wadman, J. M. Kroon, K. Bakker, R. W. A. Havenith, G. P. M. van Klink, G. van Koten, *Organometallics* **2010**, *29*, 1569.

[10] a) P. G. Bomben, K. D. Theriault, C. P. Berlinguette, *Eur. J. Inorg. Chem.* **2011**, 1806; b) K. C. D. Robson, B. D. Koivisto, A. Yella, B. Sporinova, M. K. Nazeeruddin, T. Baumgartner, M. Grätzel, C. P. Berlinguette, *Inorg. Chem.* **2011**, *50*, 5494.

[11] K.-L. Wu, C.-H. Li, Y. Chi, J. N. Clifford, L. Cabau, E. Palomares, Y.-M. Cheng, H.-A. Pan, P.-T. Chou, *J. Am. Chem. Soc.* **2012**, *134*, 7488.

[12] a) P.-T. Chou, Y. Chi, *Eur. J. Inorg. Chem.* **2006**, 3319; b) P.-T. Chou, Y. Chi, *Chem. Eur. J.* **2007**, *13*, 380.

[13] A. Hagfeldt, G. Boschloo, L. Sun, L. Kloo, H. Pettersson, *Chem. Rev.* **2010**, *110*, 6595.

[14] K.-L. Wu, H.-C. Hsu, K. Chen, Y. Chi, M.-W. Chung, W.-H. Liu, P.-T. Chou, *Chem. Commun.* **2010**, *46*, 5124.

[15] M.-W. Chung, T.-Y. Lin, C.-C. Hsieh, K.-C. Tang, H. Fu, P.-T. Chou, S.-H. Yang, Y. Chi, *J. Phys. Chem. A* **2010**, *114*, 7886.

[16] K. Funabiki, N. Noma, G. Kuzuya, M. Matsui, K. Shibata, *J. Chem. Res., Synop.* **1999**, *5*, 1301.

[17] M. K. Nazeeruddin, C. Klein, P. Liska, M. Grätzel, *Coord. Chem. Rev.* **2005**, *249*, 1460.

[18] a) C.-C. Chou, K.-L. Wu, Y. Chi, W.-P. Hu, S. J. Yu, G.-H. Lee, C.-L. Lin, P.-T. Chou, *Angew. Chem.* **2011**, *123*, 2102; b) K.-L. Wu, S.-T. Ho, C.-C. Chou, Y.-C. Chang, H.-A. Pan, Y. Chi, P.-T. Chou, *Angew. Chem. Int. Ed.* **2012**, *51*, 5642; c) C.-W. Hsu, S.-T. Ho, K.-L. Wu, Y. Chi, S.-H. Liu, P.-T. Chou, *Energy Environ. Sci.* **2012**, *5*, 7549.

[19] P.-C. Wu, J.-K. Yu, Y.-H. Song, Y. Chi, P.-T. Chou, S.-M. Peng, G.-H. Lee, *Organometallics* **2003**, *22*, 4938.

[20] K.-L. Wu, H.-C. Hsu, K. Chen, Y. Chi, M.-W. Chung, W.-H. Liu, P.-T. Chou, *Chem. Commun.* **2010**, *46*, 5124.

[21] S. E. Koops, B. C. O'Regan, P. R. F. Barnes, J. R. Durrant, *J. Am. Chem. Soc.* **2009**, *131*, 4808.

[22] S. Ito, T. N. Murakami, P. Comte, P. Liska, C. Grätzel, M. K. Nazeeruddin, M. Grätzel, *Thin Solid Films* **2008**, *516*, 4613.

[23] S. Ito, K. Nazeeruddin, P. Liska, P. Comte, R. Charvet, P. Pechy, M. Jirousek, A. Kay, S. M. Zakeeruddin, M. Grätzel, *Prog. Photovolt.: Res. Appl.* **2006**, *14*, 589.

[24] a) D. Kuang, S. Ito, B. Wenger, C. Klein, J.-E. Moser, R. Humphry-Baker, S. M. Zakeeruddin, M. Grätzel, *J. Am. Chem. Soc.* **2006**, *128*, 4146; b) Z.-S. Wang, H. Kawauchi, T. Kashima, H. Arakawa, *Coord. Chem. Rev.* **2004**, *248*, 1381.

[25] a) B. C. O'Regan, K. Walley, M. Juozapavicius, A. Anderson, F. Matar, T. Ghaddar, S. M. Zakeeruddin, C. Klein, J. R. Durrant, *J. Am. Chem. Soc.* **2009**, *131*, 3541; b) M. Miyashita, K. Sunahara, T. Nishikawa,

Y. Uemura, N. Koumura, K. Hara, A. Mori, T. Abe, E. Suzuki, S. Mori, *J. Am. Chem. Soc.* **2008**, *130*, 17874.
[26] Q. Yu, S. Liu, M. Zhang, N. Cai, Y. Wang, P. Wang, *J. Phys. Chem. C* **2009**, *113*, 14559.
[27] a) G. Boschloo, A. Hagfeldt, *Acc. Chem. Res.* **2009**, *42*, 1819; b) S. Ardo, G. J. Meyer, *Chem. Soc. Rev.* **2009**, *38*, 115; c) G. Boschloo, E. A. Gibson, A. Hagfeldt, *J. Phys. Chem. Lett.* **2011**, *2*, 3016.
[28] a) C. Klein, M. K. Nazeeruddin, P. Liska, D. Di Censo, N. Hirata, E. Palomares, J. R. Durrant, M. Grätzel, *Inorg. Chem.* **2005**, *44*, 178; b) S.-R. Jang, J.-H. Yum, C. Klein, K.-J. Kim, P. Wagner, D. Officer, M. Grätzel, M. K. Nazeeruddin, *J. Phys. Chem. C* **2009**, *113*, 1998.
[29] A. Mishra, N. Pootrakulchote, M. Wang, S.-J. Moon, S. M. Zakeeruddin, M. Grätzel, P. Bäuerle, *Adv. Funct. Mater.* **2011**, *21*, 963.
[30] a) B. C. O'Regan, K. Walley, M. Juozapavicius, A. Anderson, F. Matar, T. Ghaddar, S. M. Zakeeruddin, C. D. Klein, J. R. Durrant, *J. Am. Chem. Soc.* **2009**, *131*, 3541; b) M. Miyashita, K. Sunahara, T. Nishikawa, Y. Uemura, N. Koumura, K. Hara, A. Mori, T. Abe, E. Suzuki, S. Mori, *J. Am. Chem. Soc.* **2008**, *130*, 17874.
[31] F. Sauvage, S. Chhor, A. Marchioro, J.-E. Moser, M. Grätzel, *J. Am. Chem. Soc.* **2011**, *133*, 13103.
[32] P. Dupau, T. Renouard, H. Le Bozec, *Tetrahedron Lett.* **1996**, *37*, 7503.
[33] R. J. Sundberg, S. Jiang, *Org. Prep. Proc. Int.* **1997**, *29*, 117.
[34] B. Su, J. Zhao, Y. Cui, Y. Liang, W. Sun, *Synth. Commun.* **2005**, *35*, 2317.
[35] E. Busto, V. Gotor-Fernandez, V. Gotor, *Tetrahedron: Asymmetry* **2005**, *16*, 3427.
[36] M. J. Frisch, G. W. Trucks, H. B. Schlegel, G. E. Scuseria, M. A. Robb, J. R. Cheeseman, G. Scalmani, V. Barone, B. Mennucci, G. A. Petersson, H. Nakatsuji, M. Caricato, X. Li, H. P. Hratchian, A. F. Izmaylov, J. Bloino, G. Zheng, J. L. Sonnenberg, M. Hada, M. Ehara, K. Toyota, R. Fukuda, J. Hasegawa, M. Ishida, T. Nakajima, Y. Honda, O. Kitao, H. Nakai, T. Vreven, J. A. Montgomery, J. E. Peralta, F. Ogliaro, M. Bearpark, J. J. Heyd, E. Brothers, K. N. Kudin, V. N. Staroverov, R. Kobayashi, J. Normand, K. Raghavachari, A. Rendell, J. C. Burant, S. S. Iyengar, J. Tomasi, M. Cossi, N. Rega, J. M. Millam, M. Klene, J. E. Knox, J. B. Cross, V. Bakken, C. Adamo, J. Jaramillo, R. Gomperts, R. E. Stratmann, O. Yazyev, A. J. Austin, R. Cammi, C. Pomelli, J. W. Ochterski, R. L. Martin, K. Morokuma, V. G. Zakrzewski, G. A. Voth, P. Salvador, J. J. Dannenberg, S. Dapprich, A. D. Daniels, Farkas, J. B. Foresman, J. V. Ortiz, J. Cioslowski, D. J. Fox, *Gaussian 09, Revision A.1*, Gaussian, Inc. Wallingford, CT **2009**.
[37] X.-Z. Guo, Y.-H. Luo, Y.-D. Zhang, X.-C. Huang, D.-M. Li, Q.-B. Meng, *Rev. Sci. Instrum.* **2010**, *81*, 103106.